Electrosynthesis of nitriles from primary alcohols and ammonia on Ni catalyst

Yiying Xiao[a, b], Chia Wei Lim[b], Linfeng Gao[b], Ning Yan[*, a, b]

[a] *Joint School of National University of Singapore and Tianjin University, International Campus of Tianjin University, Binhai New City, Fuzhou 350207, China*

[b] *Department of Chemical and Biomolecular Engineering, National University of Singapore, 4 Engineering Drive 4, Singapore 117585, Singapore*

[*]Corresponding author:

Ning Yan

Email: ning.yan@nus.edu.sg

Postal address: Department of Chemical and Biomolecular Engineering, National University of Singapore, 4 Engineering Drive 4, Singapore 117585, Singapore.

Abstract

Despite the increasing interest on electrocatalytic refinery of renewable feedstocks to produce value-added chemicals, nitrile electrosynthesis from alcohols is rarely studied. Here, we report the direct electrosynthesis of nitriles from primary alcohols and ammonia, with a simple nickel catalyst under benign conditions in aqueous electrolytes. The highest benzonitrile faradaic efficiency of 63.0% was achieved at 1.375 V *vs.* RHE. The reaction proceeds via a dehydrogenation-imination-dehydrogenation sequence, with the rate-determining step likely involving the cleavage of α-carbon C-H bond of the alcohol. Based on the electrochemical and *in-situ* Raman analyses, we propose that the *in-situ* formed Ni^{2+}/Ni^{3+} redox species serves as the active site for converting alcohol to nitrile, while Ni^{2+} also exhibits capability for the oxidation of imine. Various aromatic, aliphatic and heterocyclic primary alcohols were transformed to the corresponding nitriles, exhibiting broad feasibility. This study offers a promising electrocatalytic system for the sustainable synthesis of high-value nitriles.

Keywords

nitrile, nickel catalyst, C-N coupling, electrooxidation

1. Introduction

Due to the depletable nature of fossil fuel feedstocks and the rising global emphasis on carbon neutrality, there has been an increasing interest devoted to the electrocatalytic refinery of waste materials for the sustainable synthesis of value-added chemicals.[1-3] The benefits afforded by electrocatalytic processes are multi-fold – electrical energy inputs are readily available from renewable sources, water can be used as a solvent (avoiding the need for organic solvents), and benign operations at or near ambient temperature are feasible.[4, 5] In particular, C-N coupling reactions are an important class of reactions for manufacturing various bulk and fine chemicals, such as fertilizers, synthetic fibres, pigments and pharmaceuticals.[6-8] These reactions involve the formation of carbon-nitrogen bonds between a carbon-based compound and a nitrogen source, giving rise to organonitrogen products. Notable works in electrocatalytic C-N coupling include the electrosynthesis of amines and amides from CO_2 or CO.[9-11] Interestingly, urea has been successfully synthesised from CO_2 and various nitrogenous species.[12] Recently, the valorisation of CO_2-derived formic acid and methanol to formamide has also been demonstrated.[13-15] Biomass-derived carbonyl compounds are also used for the electrocatalytic reductive amination (ERA) C-N coupling reaction.[16-18] A special case of ERA uses α-keto acids as the substrate to produce amino acids, which have immense biological uses, utilising various metal and carbon-based cathodes.[19-22]

Despite the extensive efforts in the wider topic of electrocatalytic C-N coupling, the direct electrosynthesis of nitriles from primary alcohols is not common. Nitriles are versatile intermediates for producing higher value chemicals, including biological materials, pharmaceuticals and polymers.[23, 24] The conventional chemical methods for nitrile synthesis, such as the Sandmeyer[25] and the Rosenmund-von Braun[26]

reactions, are not benign as they utilise toxic starting materials, require severe reaction conditions and generate large amounts of chemical waste (Fig. 1a). Improved chemical routes using alcohols and ammonia as the substrates, via ammoxidation[27-33] or oxidant-free dehydrogenation coupled with imination[34-36], have been recently reported. However, they face certain issues, including the need for oxidants or high reaction temperatures, as well as poor selectivity due to over-oxidation and other undesired side reactions. On the electrocatalysis front, the synthesis of hydrogen cyanide, an analogue of nitrile, has been demonstrated using methane and ammonia as the substrates,[37] albeit at elevated temperatures of 800-1000 °C with solid electrolytes. The required temperature for hydrogen cyanide synthesis in the solid electrolyte was decreased to 500-650 °C by replacing methane with methanol.[38, 39] Moreover, Zhang and co-workers have developed an efficient electro-oxidative coupling strategy for the synthesis of various nitriles with moderate to high yields from corresponding alcohols and aqueous ammonia under mild conditions.[40] Their bimetallic electrocatalyst consists of Cu and a noble metal Pd, which acted as the sites for the oxidation and coupling reactions, respectively. Therefore, opportunities exist for electrocatalytic nitrile synthesis from alcohols.

Here, we report a facile one-pot synthesis of various nitriles from primary alcohols and ammonia, in the presence of Ni catalyst under ambient temperature using aqueous electrolyte without the need for oxidants (Fig. 1b). Ten materials were first screened and Ni was determined as the optimal catalyst. Several control experiments and kinetic studies were performed to deduce the reaction pathway and rate-limiting step. To understand the metal sites contributing to the catalytic activity, we conducted electrochemical analyses and *in-situ* experiments. The influence of different reaction parameters was also studied.

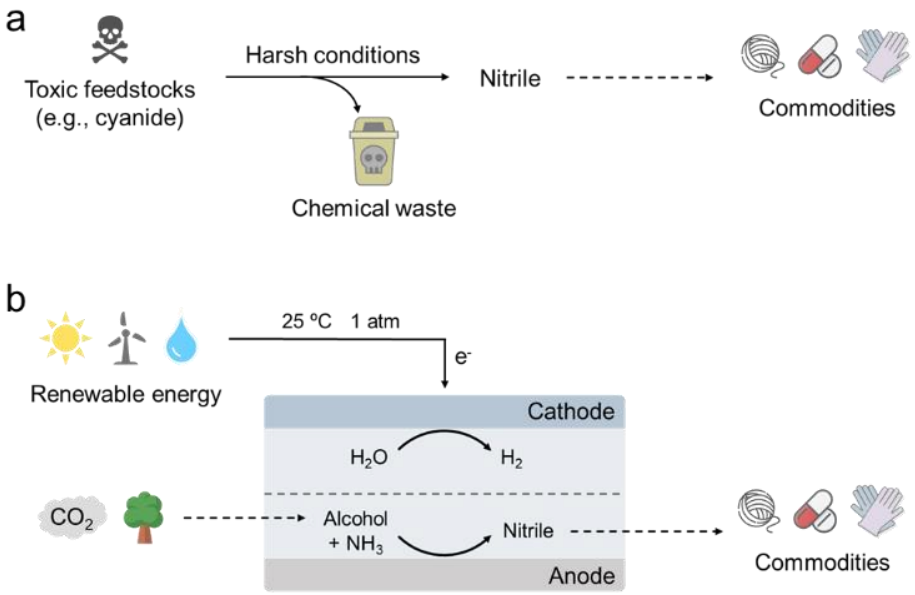

Figure 1. Schematic comparison of the nitrile syntheses. a) Conventional chemical route. **b)** Proposed electrochemical route.

2. Experimental

2.1. Chemicals

Sodium perchlorate ($NaClO_4$, ≥98.0%), sodium hydroxide (NaOH, ≥98.5%), potassium hydroxide (KOH, 90%), ammonia solution (~25 wt. % NH_3 in water), benzyl alcohol (≥99%), benzyl-α,α-d_2 alcohol (99%, D, 98%), benzaldehyde (≥99%), benzoic acid (≥99.5%), benzonitrile (≥99%), benzamide (99%), 4-methoxybenzyl alcohol (98%), 4-methoxybenzonitrile (99%), 2-hydroxybenzyl alcohol (99%), 2-hydroxybenzonitrile (99%), 4-hydroxybenzyl alcohol (99%), 4-cyanophenol (95%), 4-hydroxy-3-methoxybenzyl alcohol (98%), 4-hydroxy-3-methoxybenzonitrile (98%), 4-chlorobenzyl alcohol (99%), 4-chlorobenzonitrile (99%), 4-nitrobenzyl alcohol (99%), 4-nitrobenzonitrile (97%), 4-nitrobenzamide (98%), furfuryl alcohol (98%), 2-furonitrile (99%), acetamide (~99%), 1-butanol (99.8%), butyronitrile (≥99%), 1-hexanol (≥99%), hexanenitrile (98%), 1,6-hexanediol (99%), adiponitrile (99%), 1-pentanol (≥99%), 3-(trimethylsilyl)-1-propanesulfonic acid sodium salt (97%), hydrochloric acid (HCl, 37%) and sulfuric acid (H_2SO_4, 95.0-98.0%) were purchased from Sigma-Aldrich. Nitric acid

(HNO$_3$, 65%) and absolute ethanol (>99.7%) were provided by VWR Chemicals. Acetone (HPLC grade) and acetonitrile (HPLC grade) were purchased from Fisher Chemical. Deuterium oxide (D_2O, D, 99.9%) was purchased from Cambridge Isotope Laboratories. Nitrogen gas (N_2, 99.9995%) was supplied by Air Liquide. Commercially available reagents were used as received without further purification. All aqueous solutions were prepared using ultra-pure water (Milli-Q®, resistivity of 18.0 MΩ cm).

2.2. Preparation of electrodes

Manganese plate (Mn plate, ~1 mm thickness, 99.9%) was purchased from Xingtai Xinnai Metal Materials Co., Ltd. Iron foam (Fe foam, 1.0 mm thickness, 99.9%), cobalt foam (Co foam, 1.6 mm thickness, 99.9%), nickel foam (Ni foam, 1.0 mm thickness, ≥99.9%) and copper foam (Cu foam, 1.0 mm thickness, ≥99.7%) were purchased from Kunshan Guangjiayuan New Materials Co., Ltd. Zinc foam (Zn foam, 1.0 mm thickness, 99.9%) was purchased from Kunshan Lvchuang Electronic Tech Co., Ltd. Ruthenium plate (Ru plate, 1 mm thickness, 99.95%) was purchased from Quanzhou Qijin New Material Tech Co., Ltd. Palladium plate (Pd plate, 0.1 mm thickness, ≥99.98%) was purchased from Wuxi Mini Chemistry Art Meseum Co., Ltd. Platinum plate (Pt plate, 0.1 mm thickness, ≥99.99%) was purchased from Shanghai Chengxin Scientific Instrument Co., Ltd. Carbon paper (CP, TGP-H-060, 0.19 mm thickness) was purchased from Suzhou Sinero Tech Co., Ltd.

Fe, Co, Ni, Cu, Zn and carbon paper electrodes used in this work were cut into 1.5 × 3 cm, while the dimensions for Mn, Ru, Pd and Pt plates were 1 × 1 cm. The cleaning and preparation of metal electrodes were carried out immediately prior to use in every experiment. Fe, Zn and Mn electrodes were mechanically polished using sandpaper, then washed with ultra-pure water. Co, Ni and Cu electrodes were first sonicated with acetone for 30 min before washing with ultra-pure water, then

pretreated by immersing in 2 M HCl for 30 min. Ru, Pd and Pt electrodes were stored in 33% HNO_3 until use. The pretreatment of carbon paper was performed through sonicating in 1 M HNO_3 for 30 min. After that, the carbon paper was washed thoroughly using ultra-pure water and absolute ethanol, followed by drying overnight at 80 °C.

2.3. Material characterisation

Raman spectra were collected by a Raman microscope (XploRA^{TM} Plus, HORIBA Scientific) with a 638 nm excitation laser using a 100X objective lens. The chemical environments of the Ni foam were identified by X-ray photoelectron spectroscopy (XPS, Kratos AXIS Ultra^{DLD}, Kratos Analytical Ltd.) with mono Al Kα X-ray source. All XPS data were calibrated to C 1s (C-C bond) at 284.50 eV and analysed using XPSPEAK Version 4.1 software.

2.4. Electrochemical measurements

All the electrochemical measurements were carried out using a Gamry Interface 1010E potentiostat (Gamry Instruments Inc., U.S.). Similar to our previous study,[19] a glass two-chamber (H-type) three-electrode configurated electrochemical cell, which was separated by a piece of Nafion 117 membrane (N117, Dupont, Xianfeng Instrument Tech Co., Ltd), was used for all experiments. Reference and counter electrodes were a Hg/HgO electrode (1 M KOH) with a double-salt bridge (Shanghai Yueci Electronic Tech Co., Ltd.) and a platinum mesh (Pt mesh, 10 × 10 mm, ≥99.99%, Shanghai Chengxin Scientific Instrument Co., Ltd.), respectively. The electrolyte volume was 40 mL (50 mL in total volume) for both anodic and cathodic chambers, except for the H-cell with Mn, Ru, Pd and Pt plates as working electrodes, whose electrolyte volume was 9 mL (15 mL in total volume). In all cases, 15 mL/min purified nitrogen gas was purged through the anodic electrolyte for 30 min at the start of each experiment to exclude the air. During the measurements, the electrolyte solution was

stirred and bubbled with nitrogen gas continuously. The potentials applied against the Hg/HgO reference electrode were calibrated to the reversible hydrogen electrode (RHE) scale without iR compensation using the follow equation:

$$E_{\mathrm{RHE}}(\mathrm{V}) = E_{\mathrm{Hg/HgO}}(\mathrm{V}) + 0.098\ \mathrm{V} + 0.059\ \mathrm{V} \times \mathrm{pH} \qquad \text{(eq. 1)}$$

All current densities were calculated on the basis of the measured currents and geometric areas of the working electrodes (4.5 cm^2 for Fe, Co, Ni, Cu, Zn foams and carbon paper, 1 cm^2 for Mn, Ru, Pd and Pt plates).

The electrosynthesis of nitriles was performed by chronoamperometry and investigated systematically under different working electrodes, applied potentials, pH, substrate concentrations, ammonia concentrations and substrate types. In a typical electrolysis procedure, certain concentrations of NH_3, $NaClO_4$, KOH and/or NaOH aqueous solution with and without organic substances were used as the anolyte and catholyte, respectively. Specifically, the influence of pH on the catalytic performance was carried out by varying the concentrations of NaOH and/or $NaClO_4$ to reach the desired pH values and keep the total molar of the anions in different electrolytes was the same.

The linear sweep voltammetry (LSV) measurements were performed at a scan rate of 5 mV/s or 10 mV/s under various conditions.

The cyclic voltammetry (CV) measurements were conducted with scan rates ranging from 5 to 200 mV/s under various conditions.

2.5. Product identification and quantification

During and after the chronoamperometry test, the electrolyte solution collected from the anodic chamber was immediately analyzed by either high-performance liquid chromatography (HPLC), gas chromatography (GC) or ^1H nuclear magnetic

resonance (NMR) spectroscopy depending on the substrate type. The cathodic electrolyte was also analyzed to make sure the membrane was in good condition. Before HPLC and GC analyses, the electrolyte solution was acidified to pH 5−6 by 2 M HCl and filtered through a polyethersulfone (PES) syringe filter (0.22 μm, Microlab Scientific).

The aromatic and heterocyclic compounds were analyzed by HPLC (Agilent, 1260 Infinity II), equipped with an InfinityLab Poroshell 120 EC-C18 column (3.0 × 150 mm, 2.7-Micron, 1000 bar) and an ultraviolet-visible (UV) detector (1260 Infinity II Refractive Index detector). 5 mM H_2SO_4 aqueous solution and acetonitrile with 0.2 mL/min flow rate (isocratic elution) were used as the A and B mobile phases, respectively. The column temperature was 30 °C and the injection volume was 3 μL.

The aliphatic substrates (except for ethanol and 1,6-hexanediol) and their derivatives were determined by GC (Agilent, 7890A), equipped with a HP-5 column (30 m × 0.320 mm, 0.25 micron) and a flame ionization detection (FID) detector. Nitrogen was applied as the carrier gas. 1-Pentanol was added in the previously prepared 2 M HCl (used for acidifying the samples) as the internal standard to quantify the substrates, intermediates and products.

The qualitative and quantitative analyses of ethanol, 1,6-hexanediol and their derivatives were carried out by NMR spectroscopy (Bruker Ascend^{TM} 400, 400 MHz) at room temperature with water suppression. In short, 250 μL of the sampled electrolyte solution was mixed with 250 μL of internal standard solution consisting 3-(trimethylsilyl)-1-propanesulfonic acid sodium salt in D_2O.

The Faradaic efficiency (FE) for target products, side products and intermediates was calculated as follows:

$$\mathrm{FE}(\%) = \frac{n \times C \times V \times F}{Q} \times 100 \qquad \text{(eq. 2)}$$

where *n* is the number of electrons required for the formation of the compound (*n* = 2 for aldehyde; *n* = 4 for nitrile, amide and acid), *C* is the molar concentration of the compound, *V* is the volume of the electrolyte, *F* is the Faraday constant (96485 C mol^{-1}), and *Q* represents the total charge passed during the electrolysis.

2.6. Kinetic modelling of the reaction

A set of time-dependent concentrations of benzyl alcohol, benzaldehyde, benzonitrile and benzoic acid were used to simulate the reaction rate constants. Reaction kinetic parameters were fitted according to the least squares fitting algorithm of MATLAB lsqcurvefit.[41-43] Several constrains were used to confirm that the fitting curve is reasonable. The kinetic equations and fitting curve are shown in Supplementary Fig. S18.

2.7. In-situ Raman spectroscopy measurements

A home-made electrochemical cell shown in Supplementary Fig. S10 was used for *in-situ* Raman spectroscopy experiments. *In-situ* Raman spectra were recorded using the aforementioned Raman microscope (XploRA^{TM} Plus, HORIBA Scientific), with a 638 nm excitation laser and a 10X objective lens, under controlled potentials by the electrochemical workstation (Gamry Interface 1010E potentiostat, Gamry Instruments Inc., U.S.). Further details for the setup and measurements are provided in Supplementary Fig. S10.

3. Results and Discussion

3.1. Ni is the best catalyst among the screened materials

In the initial screening, nine monometallic catalysts which were reported to be active in the thermocatalytic nitrile production from alcohols, including Zn, Mn, Fe, Co, Ni,

Cu, Ru, Pd and Pt,[44] as well as carbon paper were studied using benzyl alcohol (BnOH) as a model compound (Fig. 2a). The experiment using Zn was not successful as Zn actively reacted with alkali to release hydrogen. For the other nine materials, Ni delivers benzonitrile (PhCN) as the main product with the highest faradaic efficiency (FE) of 49.2% and formation rate of 90.8 mmol m^{-2}_{cat} h^{-1}, with the co-generation of benzaldehyde (PhCHO), benzoic acid (PhCOOH) and benzamide ($PhCONH_2$). Ru also has the capacity for PhCN production, but a significantly lower nitrile FE of 11.2% and an unexpectedly low total FE for the organic products (25.6%) were observed. These are possibly due to the competing ammonia oxidation reaction[45] and dissolution of Ru under oxidative potentials (as indicated by the dark green-coloured electrolyte). In sharp contrast, Mn, Fe, Co, Cu, Pd, Pt, and C show no activity for PhCN production. Particularly, Mn, Co and Cu faced severe issues of metal oxidation and leaching under the reaction conditions. We further investigated the electrocatalytic properties of the catalysts using linear sweep voltammetry (LSV) (Supplementary Fig. S1), and conducted the electro-oxidation of BnOH without the addition of ammonia (Fig. 2b). In addition to Ni, Ru, Co and Cu also exhibit activity in converting BnOH to the corresponding oxidative products, with a consumption rate of up to 946.7 mmol m^{-2}_{cat} h^{-1} on Ru. However, the total FEs on Co, Cu and Ru are unsatisfactory, with only 50.3% for Ru and less than 15% for Co and Cu. In the absence of BnOH, for Mn, Co, Ni, Cu and Ru, there exist anodic currents before the operating potentials (1.425 V or -0.265 V *vs.* RHE), likely due to metal oxidation (Supplementary Fig. S1a-e). Contrary to Ni and Ru which display LSV current enhancements in the presence of BnOH, Mn, Co and Cu show decreased peak currents, suggesting that the BnOH oxidation rates are very slow on these metals. For Mn, Co, and Cu, it may be beneficial to dope

another element to stabilise the higher oxidation state metal species, thus reducing the metal dissolution rates.[15, 40, 46]

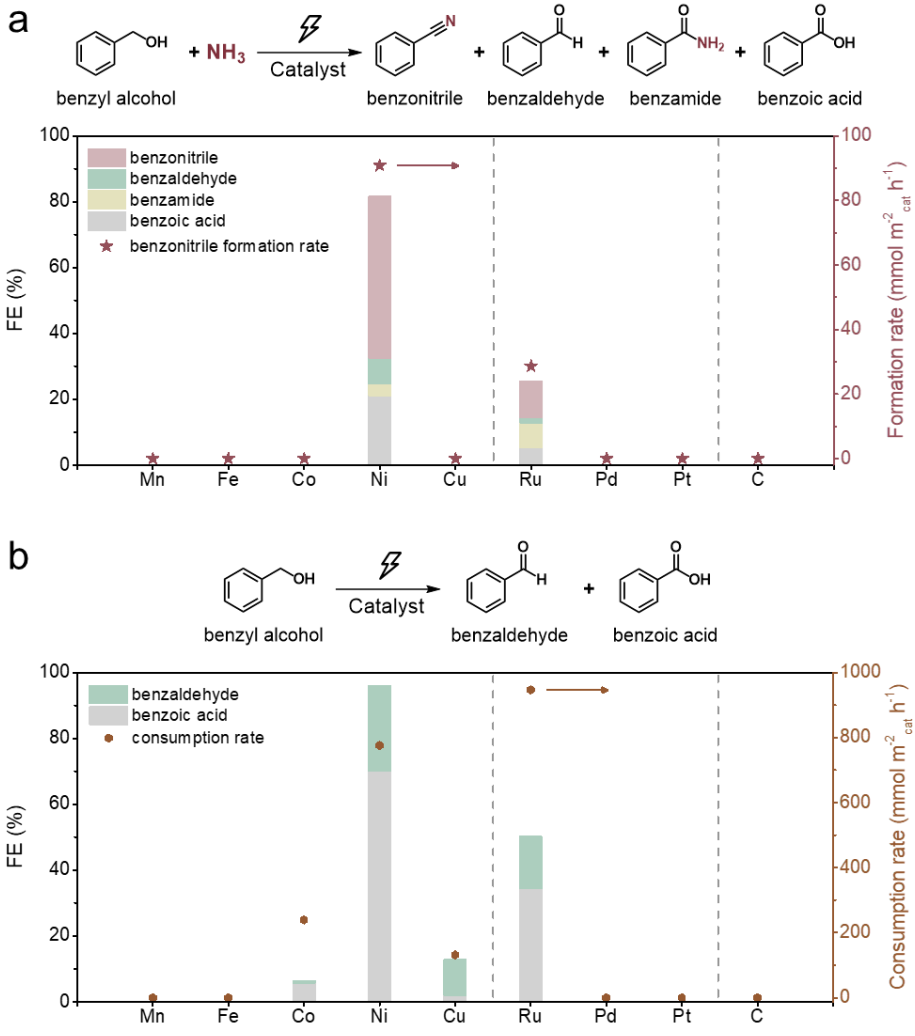

Figure 2. Catalyst screening and performance analysis. a) FEs and PhCN formation rate of electro-oxidative coupling of BnOH and NH_3 on various catalysts. Reaction conditions: 20 mM BnOH, 1 M NH_3, pH 13, 1.425 V *vs.* RHE (0.675 V *vs.* RHE for Mn), 8 h reaction time (reduced for Co and Cu due to significant metal dissolution). **b)** FEs and BnOH consumption rate of electro-oxidation of BnOH on various catalysts. Reaction conditions: 20 mM BnOH, pH 13, 1.425 V *vs.* RHE (-0.265 V *vs.* RHE for Mn), 1 h reaction time.

3.2. Nitrile synthesis follows a dehydrogenation-imination-dehydrogenation sequence

In thermocatalysis, there are two possible reaction pathways for nitrile synthesis from primary alcohols and ammonia (Scheme S1).[35] Pathway I starts with the

dehydrogenation of alcohol to aldehyde, which then condenses with ammonia to form an imine intermediate. The imine is subsequently dehydrogenated to afford the nitrile product. In pathway II, a direct nucleophilic attack by an ammonia molecule on the α-carbon of the alcohol occurs. This results in an S_N2 substitution of the -OH group with -NH_2 group to produce an amine intermediate, which then undergoes sequential dehydrogenations to generate a nitrile product.

A series of control experiments were carried out to determine the main pathway (Table 1). No PhCN was detected in the absence of applied potential, BnOH or ammonia (Entries 1-3), and only the oxidative products of BnOH were generated when ammonia was absent, confirming that PhCN originates from the electro-oxidative coupling of BnOH and ammonia. Notably, when BnOH was replaced by PhCHO, PhCN could be obtained with similar FE of ~50% (Entry 5), demonstrating that PhCHO serves as the key intermediate for nitrile production. We also employed benzylamine ($BnNH_2$) as the carbon source, considering that nitrile could be synthesised from the electrochemical dehydrogenation of amine on Ni-based catalysts.[47-56] Indeed, the electro-oxidation of $BnNH_2$ resulted in PhCN formation, though the FE (74.5%) was rather different from that when using BnOH as the carbon source (Entry 6). Moreover, we were not able to detect $BnNH_2$ intermediate throughout the whole process of BnOH electrolysis (Supplementary Fig. S2, S3a). These results suggest that pathway II via the direct amination of BnOH to yield $BnNH_2$ is highly unlikely.

Table 1. The list of control experiments to confirm the reaction pathway.

Entry	C source	N source	*E* / V *vs.* RHE	Main organic product (FE / %)
1	BnOH	NH_3	×	N.D.
2	×	NH_3	1.425	N.D.
3	BnOH	×	1.425	PhCOOH (94.0)
4	BnOH	NH_3	1.425	PhCN (49.2)
5	PhCHO	NH_3	1.425	PhCN (46.2)
6	$BnNH_2$	NH_3	1.425	PhCN (74.5)
7	PhCN	NH_3	1.425	$PhCONH_2$
8	PhCOOH	NH_3	1.425	N.D.
9	$PhCONH_2$	NH_3	1.425	N.D.

Reaction conditions: Ni foam, 20 mM C source (if present), 1 M N source (if present), pH 13, 1.425 V *vs.* RHE (if present), 8 h reaction time. N.D. = not detected.

To probe the possibility of the various side reactions, PhCN, PhCOOH and $PhCONH_2$ were used to conduct the electrolysis. When PhCN was used as the carbon source, only a trace amount of $PhCONH_2$ was detected, with a $PhCONH_2$ to PhCN ratio of less than 4.5% (Entry 7, Supplementary Fig. S3b, c), which is smaller than the corresponding ratio during BnOH electrolysis (7-8%). This implies that $PhCONH_2$ is probably produced from PhCN hydrolyzation as well as hemiaminal ($PhC(OH)NH_2$) dehydrogenation. Electrolysis using PhCOOH and $PhCONH_2$ failed to generate any organic products (Entries 8, 9). Taken together, the electrocatalytic synthesis of nitrile using primary alcohol and ammonia follows a dehydrogenation-imination-dehydrogenation pathway (Scheme 1). The direct oxidation of aldehyde to form acid serves as the main competing reaction, and the dehydrogenation of hemiaminal intermediate and hydrolyzation of nitrile lead to the amide side product.

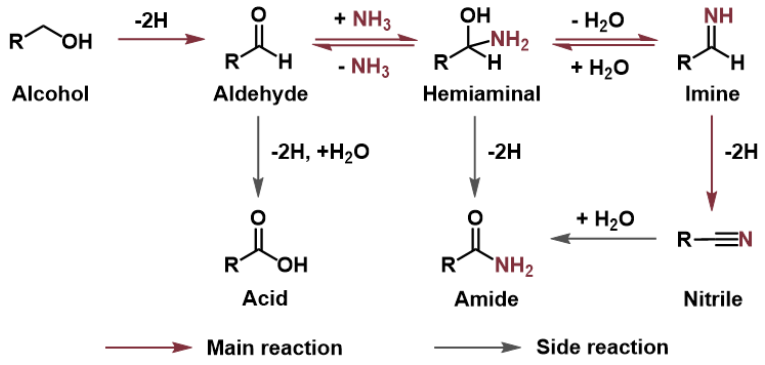

293

294 **Scheme 1.** Plausible reaction pathway in the Ni foam catalysed electro-oxidative coupling of primary
295 alcohols and ammonia to nitriles.

296 ***3.3. Ni^{2+}/Ni^{3+} redox cycle and Ni^{2+} are active for nitrile synthesis***

297 We initially used LSV to examine the electrochemical properties of Ni foam. In the
298 absence of the organic compounds or ammonia, there is an oxidation peak with an
299 onset at ~1.35 V *vs.* RHE, which is ascribed to the transformation of Ni^{2+} to Ni^{3+} (Fig.
300 3a, b, eq. 3).

$$Ni(OH)_2 + OH^- \rightleftharpoons NiOOH + H_2O + e^- \quad \text{(eq. 3)}$$

301 When ammonia is present, the current starts to climb in the same potential region
302 (Supplementary Fig. S4), attributable to the Ni^{3+}-catalysed direct oxidation of
303 ammonia.[57] Upon the addition of BnOH, Ni foam exhibits an oxidative wave with
304 enhanced current density (Fig. 3a), which is also observable in the cyclic voltammetry
305 (CV) curves (Supplementary Fig. S5a). Furthermore, the reduction peak
306 corresponding to the conversion of Ni^{3+} to Ni^{2+} is weakened after introducing BnOH
307 (Supplementary Fig. S5a). A similar phenomenon was observed from the multi-
308 potential chronoamperometry tests, displaying that the reduction current of Ni^{3+} to Ni^{2+}
309 disappeared when BnOH was injected during the open circuit state (Supplementary
310 Fig. S6). We used *ex-situ* X-ray photoelectron spectroscopy (XPS) and Raman
311 spectroscopy to understand this process. As illustrated in the XPS spectra, the surface
312 of the acid-treated Ni foam was mainly composed of metallic Ni and Ni^{2+}

(Supplementary Fig. S7b). When the organic compounds and ammonia were absent, the characteristic peaks associated with Ni^{3+} were detected in both XPS and Raman spectra after applying a potential of 1.45 V *vs.* RHE (Supplementary Fig. S7c, S8), which disappeared upon stirring in an electrolyte solution containing BnOH and ammonia (Supplementary Fig. S7d, S8). According to the above results, we deduce that the electrochemically generated Ni^{3+} triggers the C-N coupling of BnOH and ammonia to PhCN, accompanied by the simultaneous reduction of Ni^{3+} to Ni^{2+} (Supplementary Fig. S9, eq. 4), which is likely the widely accepted Ni^{2+}/Ni^{3+}-mediated indirect oxidation of organic compounds.[58]

$$4NiOOH + BnOH + NH_3 \rightarrow 4Ni(OH)_2 + PhCN + H_2O \qquad \text{(eq. 4)}$$

In-situ Raman analyses (Supplementary Fig. S10) were further carried out to verify the assumption through probing the changes in Ni foam during potential alterations. As displayed in Fig. 3c, two peaks located at 473 and 553 cm^{-1} are observed above around 1.35 V *vs.* RHE, which correspond to the Ni^{3+}-O bending and stretching vibrations of NiOOH, respectively. The intensities of the NiOOH peaks increase progressively as the potential becomes more positive. The presence of ammonia has insignificant effects on the formation of NiOOH: it only results in slightly decreased peak intensities (Supplementary Fig. S11, S12), possibly due to the partial passivation of the electrode surface by ammonia. When BnOH was added, the NiOOH peaks only accumulate at potentials higher than 1.55 V *vs.* RHE, with distinctly decreased intensities (Fig. 3d). These results confirm that the *in-situ* formed Ni^{2+}/Ni^{3+} redox species serves as the active site for the PhCN production from BnOH and ammonia.

Interestingly, compared to that with BnOH and ammonia, the NiOOH peaks start to appear at a negatively shifted potential (~1.45 V *vs.* RHE) with higher intensities

when PhCHO intermediate and ammonia are present (Fig. 3e). This is despite a higher current recorded under the *in-situ* Raman measurements (Supplementary Fig. S13), which may imply that the reaction between PhCHO and NiOOH is faster (compared to that between BnOH and NiOOH) and the peaks may be expected to emerge at a more positive potential. Additionally, there is indeed an obvious increase in the Ni^{2+}/Ni^{3+} oxidative current (Fig. 3b, Supplementary Fig. S5b), as well as a decrease in the Ni^{3+}/Ni^{2+} reductive current (Supplementary Fig. S5b) after adding PhCHO. The characteristic peaks attributed to Ni^{3+} were also not discernible after mixing the oxidative-potential-treated Ni foam with PhCHO and ammonia (Supplementary Fig. S7e, S8). Thus, these give us hints that the Ni^{2+}/Ni^{3+} species may be just one of the several possible reactive sites for the C-N coupling of PhCHO and ammonia. Remarkably, given that the onset potential shifts largely in the negative direction to around 1.23 V *vs.* RHE when PhCHO is present (Fig. 3b), it is reasonable to speculate that Ni^{2+} also plays a key role in the oxidative coupling reaction (eq. 5).

$$PhCHO + NH_3 + 2OH^- \xrightarrow{Ni^{2+}} PhCN + 3H_2O + 2e^- \quad \text{(eq. 5)}$$

To confirm this, we performed electrolysis in the presence of PhCHO and ammonia at 1.27 V *vs.* RHE (Supplementary Fig. S14), where Ni^{3+} does not form (Supplementary Fig. S15, S16). Although at a relatively lower formation rate, PhCN is the only detectable product with a high FE of 74.8%, demonstrating the promising potential of the Ni^{2+} site in the production of nitriles from aldehydes and ammonia. We note that Ni^{2+} has only been hinted, based on LSV studies, as the active site for limited cases of electrochemical oxidative reactions, including cysteine (CySH) dimerisation[59, 60] and N-acetylglucosamine (NAG) oxidation[61] reactions.

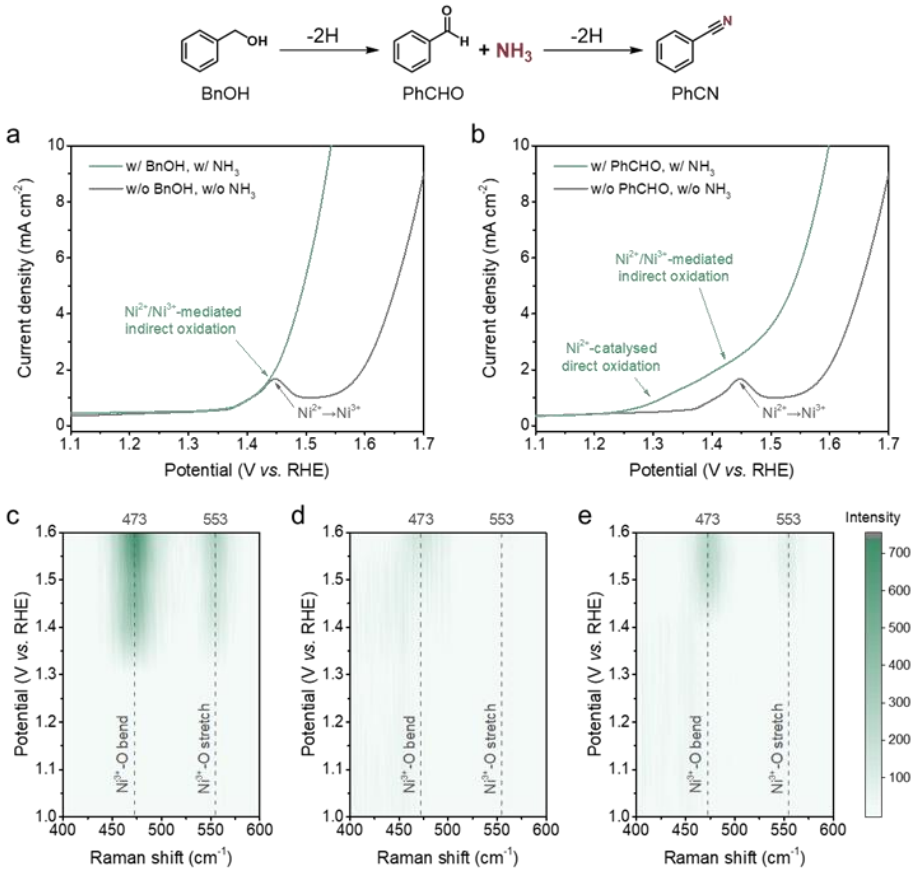

Figure 3. Investigation of the catalytic active sites. a) LSV curves of Ni foam without (grey line) and with (green line) BnOH and NH_3 at a scan rate of 10 mV/s without stirring (pH 13). **b)** LSV curves of Ni foam without (grey line) and with (green line) PhCHO and NH_3 at a scan rate of 10 mV/s without stirring (pH 13). 2D spectra for the potential-dependent *in-situ* Raman studies of Ni foam **c)** without BnOH, PhCHO or NH_3; **d)** with BnOH and NH_3 and **e)** with PhCHO and NH_3. Further details for Raman spectra are given in Supplementary Fig. S12.

3.4. Nitrile synthesis depends on potentials, pH and reactant concentrations

The effects of various applied potentials, pH values and ammonia/BnOH concentrations on the FEs and PhCN formation rate of the Ni foam-catalysed electrosynthesis of PhCN were systematically investigated. As the potential becomes more positive than ~1.42 V *vs.* RHE, the PhCN formation rate increases sharply from around 40 to 90 mmol m^{-2}_{cat} h^{-1} and levels off (Fig. 4a), which could be rationalised by earlier LSV results (Fig. 3a). As long as the NiOOH active phase could be rapidly regenerated under these sufficiently positive potentials, the rate of the Ni^{2+}/Ni^{3+}-mediated indirect oxidation of BnOH and ammonia is independent of the applied

potentials, which also suggests that the rate-determining step (RDS) directly involves the PhCN formation as opposed to the generation of NiOOH. In the range of 1.35 to 1.50 V *vs.* RHE, the FE towards PhCN firstly increases to its highest value of 63.0% and shows a downward trend at potentials higher than 1.375 V *vs.* RHE.

Notably, the PhCN formation rate exhibits a strong pH dependence, increasing substantially from 0.66 mmol m^{-2}_{cat} h^{-1} (pH 12) to 90.8 mmol m^{-2}_{cat} h^{-1} (pH 13) and declining greatly thereafter (Fig. 4b). The very low PhCN formation rate at pH 12 is likely due to the lack of formation and/or regeneration of NiOOH caused by insufficient OH^- as indicated in eq. 3. Possible reasons for the drops in PhCN formation rate and FE at pH 14 include that (1) the imine formation is suppressed while the geminal diol formation is promoted on account of more prevalent nucleophilic attack by OH^- on imine and aldehyde (Scheme S2);[62] and (2) strong alkaline electrolyte is beneficial for the Cannizzaro reaction and the hydrolysis of nitrile (Scheme S3), leading to the enhancement of acid formation. The lower FE for PhCN at pH 14, in contrast to that at pH 13, is also observed regardless of the ammonia concentrations tested (Fig. 4c). As the ammonia concentration increases, the PhCN FE displays a significant increase, possibly owing to the shifted aldehyde-imine equilibrium to the imine side. There is a decline of FE for PhCN at high ammonia concentrations, probably because ammonia oxidation reaction becomes more favourable. When the BnOH concentration increases, the formation rate and FE of PhCN show remarkable upward trends before being subject to fluctuations (Fig. 4d). The plateau in the PhCN formation rate at BnOH concentrations above 20 mM may be attributed to the saturation of the Ni^{3+} sites, whose rate of transformation from Ni^{2+} now limits the overall rate of PhCN formation.

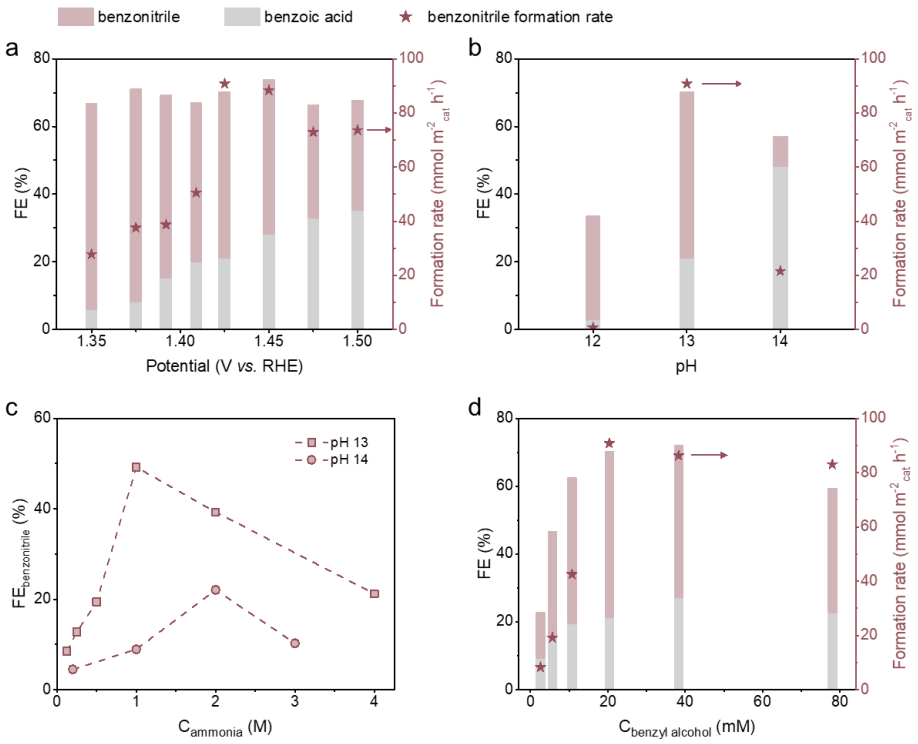

Figure 4. Influence of reaction conditions on PhCN electrosynthesis. FEs and PhCN formation rate of the electro-oxidative coupling of BnOH and NH_3 on Ni foam for 8 h under different **a)** applied potentials (20 mM BnOH, 1 M NH_3, pH 13) and **b)** pH values (20 mM BnOH, 1 M NH_3, 1.425 V *vs.* RHE. **c)** FE of PhCN in the Ni foam catalysed electro-oxidative coupling of BnOH and NH_3 for 8 h under different ammonia concentrations (20 mM BnOH, 1.425 V *vs.* RHE). **d)** FEs and PhCN formation rate of the electro-oxidative coupling of BnOH and NH_3 on Ni foam for 8 h under different BnOH concentrations (1 M NH_3, pH 13, 1.425 V *vs.* RHE).

3.5. The rate-determining step involves the alcohol α-carbon C-H bond cleavage

Kinetic analyses were carried out to further understand the RDS of the reaction at pH 13 and 1.425 V *vs.* RHE. The formation of PhCN was first order with respect to BnOH at low concentrations, attaining an approximately zeroth-order dependence at BnOH concentrations beyond 20 mM. (Fig. 5a). Similarly, a roughly first-order dependence on ammonia concentration was determined at lower concentrations, whereas a negative order was obtained above 1 M NH_3 (Fig. 5b). The negative order could be rationalised by the ammonia poisoning effect, which is also revealed in the correlation between BnOH consumption rate and ammonia concentration (Supplementary Fig. S17).

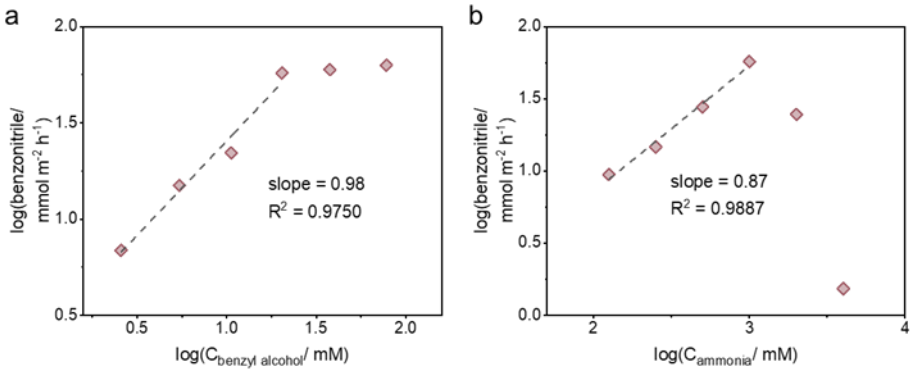

Figure 5. Kinetic measurements of PhCN electrosynthesis. The dependences of PhCN formation rate on the concentration of **a)** BnOH (1 M NH_3) and **b)** NH_3 (20 mM BnOH) at pH 13, 1.425 V *vs.* RHE and conversion around 20%.

On the basis of the proposed reaction pathway (Scheme 1) and observed reaction orders, we conducted kinetic modelling of the reaction (Supplementary Fig. S18) to fit the experimental results as depicted in Supplementary Fig. S3a. Due to the limited concentration of the $PhCONH_2$ side product throughout the period of reaction (< 3% yield), a simplified reaction scheme (Scheme 2) was used. The kinetic model predictions agree reasonably well with the experimental results and the optimised parameters are displayed in Table 2, where k_1, k_2 and k_3 refer to the rate constants for the production of PhCHO, PhCN and PhCOOH, respectively, while K is the equilibrium constant for the reversible reaction between PhCHO and imine. Although these rate constants have the same order of magnitude, the fact that k_1 has the lowest value implies that the RDS may involve the dehydrogenation of BnOH to form PhCHO.

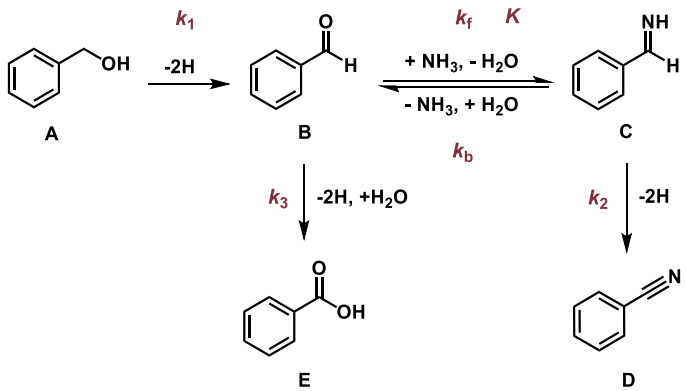

Scheme 2. Simplified reaction pathway used for the modelling of the Ni foam catalysed benzonitrile synthesis from benzyl alcohol and ammonia.

Table 2. Kinetic modelling of the reaction rate constants (k_i) and equilibrium constant (K).

k_1 / h^{-1}	k_2 / h^{-1}	k_3 / h^{-1}	K / mM^{-1}
0.211	0.479	0.243	1.15×10^{-3}

Reaction conditions: Ni foam, 20 mM BnOH, 1 M NH_3, pH 13, 1.425 V *vs.* RHE.

A kinetic isotope effect (KIE) study was performed to determine whether the RDS is the C-H bond cleavage at the α-carbon or the O-H bond breakage in the hydroxyl group of BnOH. The undeuterated substrate ($PhCH_2OH$) and $PhCD_2OH$ (deuteration of both α-hydrogen of benzyl alcohol) were transformed to PhCN under the same reaction conditions. As exhibited in Table 3, the formation rate of $PhCD_2OH$ is smaller than that of $PhCH_2OH$, yielding a KIE value of 1.73. The observed normal KIE value suggests that the α-hydrogen abstraction through a hydrogen atom transfer mechanism may indeed be the RDS for the overall reaction (eq. 6).

$$(PhCH_2OH)_{ads} + NiOOH \xrightarrow{RDS} (Ph\dot{C}HOH)_{ads} + Ni(OH)_2 \qquad \text{(eq. 6)}$$

It is worth mentioning that Choi *et al.* have demonstrated another novel mechanism involving hydride transfer from α-hydrogen in alcohols to Ni^{4+} site in NiOOH.[63, 64] Considering that this mechanism happens at more positive potentials (> 1.5 V *vs.* RHE) and is potential-dependent with the regeneration of the catalytically active species as the RDS, we rule out the possibility of this pathway in our case.

448 **Table 3.** Kinetic isotopic effects for PhCN electrosynthesis.

Entry	Alcohol	PhCN formation rate / mmol m^{-2}_{cat} h^{-1}	KIE
1	$PhCH_2OH$	57.3	
2	$PhCD_2OH$	33.2	
3	$k_{PhCH_2OH}/k_{PhCD_2OH}$		1.73

Reaction conditions: Ni foam, 20 mM $PhCH_2OH$ or $PhCD_2OH$, 1 M NH_3, pH 13, 1.425 V *vs.* RHE, around 20% conversion.

449 ***3.6. Electrosynthesis on Ni extends to other nitriles***

450 A series of aromatic, aliphatic and heterocyclic primary alcohols were used as
451 substrates to study the performance of our electrocatalytic system at synthesising the
452 corresponding nitriles. Initially, we used aromatic substrates with electron-donating
453 groups at the para- or ortho-position, including 4-methoxybenzyl alcohol, 4-
454 hydroxybenzyl alcohol, 2-hydroxybenzyl alcohol and vanillyl alcohol, which gave very
455 low to negligible conversions (Supplementary Table S1). Based on literature[65, 66]
456 and our LSV analysis (Supplementary Fig. S19), a probable reason for the inactivity
457 is the passivation of the Ni foam brought about by a radical polymerisation process,
458 as the substituents may be converted to negatively charged phenoxide ions under
459 alkaline reaction conditions. Among the aromatic substrates para-substituted with
460 electron-withdrawing groups (-Cl and $-NO_2$), the conversions are relatively high (above
461 87%), although the nitrile selectivities are lower than that obtained using BnOH as the
462 substrate (Fig. 6). This is mainly due to much higher amide selectivities (compared to
463 that of using BnOH as substrate) on these substituted substrates (Supplementary
464 Table S2). Similar phenomena of depressed nitrile selectivity and high amide
465 selectivity were seen when using furfuryl alcohol as the substrate. Interestingly, the 2-
466 furonitrile was observed to convert rapidly to the amide on standing, within several

hours even without stirring. Remarkably, the Hammet plot (Supplementary Fig. S20) exhibits a good linear correlation with a positive slope,[67] implying that the rate-determining alcohol dehydrogenation step involves more proton-transfer than electron-transfer character.[68, 69] Meanwhile, the aliphatic alcohols could also be transformed to corresponding nitriles, albeit with lower selectivities. As a majority of these substrates have been reported to be derivable from lignocellulose and/or CO_2,[70-76] our electrosynthetic strategy shows promising feasibility at valorising waste materials to make organonitrogen products.

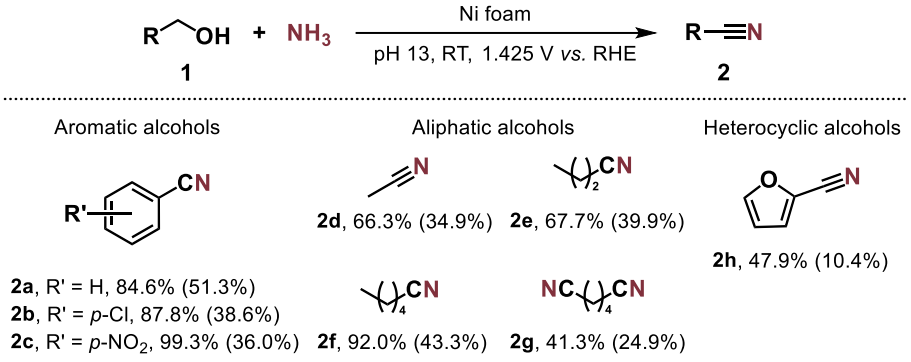

Figure 6. Substrate scope of the electrosynthesis of nitriles from primary alcohols and ammonia. Reaction conditions: Ni foam, 20 mM primary alcohol (5 mM for **1b** and **1c**), 1 M NH_3, pH 13, 1.425 V *vs.* RHE, 8 h reaction time. Conversions and selectivities are indicated below each compound, with the latter in parentheses.

4. Conclusions

We have utilised Ni foam for the electrocatalytic synthesis of benzonitrile from benzyl alcohol, with the highest formation rate of 90.8 mmol m^{-2}_{cat} h^{-1} and FE of 63.0%. The reaction likely follows a dehydrogenation-imination-dehydrogenation pathway, with the oxidation of the aldehyde intermediate to carboxylic acid being the main competing reaction and amide as another side product. Ni^{2+}/Ni^{3+} redox species acts as a key site for the C-N coupling between benzyl alcohol and ammonia to produce benzonitrile. The kinetic studies revealed that the extraction of the α-hydrogen from the primary alcohol via a hydrogen atom transfer mechanism is likely the overall rate-limiting step.

Notably, we showed that Ni^{2+} is a plausible site for the oxidative coupling, specifically for the oxidation of imine to nitrile, which has not been reported so far. In all, we have demonstrated a noble-metal-free monometallic catalyst for the electrocatalytic nitrile synthesis from primary alcohols. Given the established electrocatalytic pathways from nitrogen-containing ions present in wastewater (NO_3^-, NO_2^-) to NH_3, our work is potentially an enabler of the environmentally sustainable electrosynthesis of valuable nitrile compounds purely using waste materials (CO_2, waste biomass, wastewater) as feedstocks.

Data Availability

All the data used to support the findings of this study are included in this paper and its supplementary information file.

Statement of Competing Interests

The authors declare no competing interests.

Author Contributions

N.Y.: Conceptualization, Formal Analysis, Resources, Writing – Review & Editing, Supervision, Funding Acquisition. **Y.X.:** Conceptualization, Methodology, Formal Analysis, Investigation, Writing – Original Draft, Writing – Review & Editing, Visualization. **C.W.L.:** Formal Analysis, Investigation, Writing – Original Draft, Writing – Review & Editing. **L.G.:** Methodology, Formal Analysis, Writing – Review & Editing.

Funding Sources

This work was supported by the National Research Foundation Singapore NRF Investigatorship (Award No. NRF-NRFI07–2021–0006).

Acknowledgement

We appreciate Dr. Zeliang Yuan for performing XPS measurements. We express our gratitude to Professor Kang Zhou for helping with the fabrication of *in-situ* Raman electrochemical cell.

References

[1] J.G.J. Olivier, J.A.H.W. Peters, G. Janssens-Maenhout, Trends in global CO_2 emissions. 2012 Report, Netherlands, 2012. https://doi.org/10.2788/33777.
[2] C. Tang, Y. Zheng, M. Jaroniec, S.-Z. Qiao, Electrocatalytic Refinery for Sustainable Production of Fuels and Chemicals, Angew. Chem. Int. Ed. 60 (2021) 19572-19590. https://doi.org/10.1002/anie.202101522.
[3] C. Tang, Q. Zhang, Green Electrification of the Chemical Industry Toward Carbon Neutrality, Engineering (2023). https://doi.org/10.1016/j.eng.2023.04.018.
[4] D. Bogdanov, M. Ram, A. Aghahosseini, A. Gulagi, A.S. Oyewo, M. Child, U. Caldera, K. Sadovskaia, J. Farfan, L. De Souza Noel Simas Barbosa, M. Fasihi, S. Khalili, T. Traber, C. Breyer, Low-cost renewable electricity as the key driver of the global energy transition towards sustainability, Energy 227 (2021) 120467. https://doi.org/10.1016/j.energy.2021.120467.
[5] S. Chu, Y. Cui, N. Liu, The path towards sustainable energy, Nat. Mater. 16 (2017) 16-22. https://doi.org/10.1038/nmat4834.
[6] J. Li, Y. Zhang, K. Kuruvinashetti, N. Kornienko, Construction of C–N bonds from small-molecule precursors through heterogeneous electrocatalysis, Nat. Rev. Chem. 6 (2022) 303-319. https://doi.org/10.1038/s41570-022-00379-5.
[7] N. Kurig, R. Palkovits, Electrochemical nitration for organic C–N bond formation: a current view on possible N-sources, mechanisms, and technological feasibility, Green Chem. 25 (2023) 7508-7517. https://doi.org/10.1039/D3GC02084C.
[8] P. Liao, J. Kang, R. Xiang, S. Wang, G. Li, Electrocatalytic Systems for NO_x Valorization in Organonitrogen Synthesis, Angew. Chem. Int. Ed. 63 (2024) e202311752. https://doi.org/10.1002/anie.202311752.
[9] Y. Wu, Z. Jiang, Z. Lin, Y. Liang, H. Wang, Direct electrosynthesis of methylamine from carbon dioxide and nitrate, Nat. Sustain. 4 (2021) 725-730. https://doi.org/10.1038/s41893-021-00705-7.
[10] M. Jouny, J.-J. Lv, T. Cheng, B.H. Ko, J.-J. Zhu, W.A. Goddard, F. Jiao, Formation of carbon–nitrogen bonds in carbon monoxide electrolysis, Nat. Chem. 11 (2019) 846-851. https://doi.org/10.1038/s41557-019-0312-z.
[11] J. Li, N. Kornienko, Electrochemically driven C–N bond formation from CO_2 and ammonia at the triple-phase boundary, Chem. Sci. 13 (2022) 3957-3964. https://doi.org/10.1039/D1SC06590D.

[12] Y. Wang, D. Chen, C. Chen, S. Wang, Electrocatalytic Urea Synthesis via C–N Coupling from CO_2 and Nitrogenous Species, Acc. Chem. Res. 57 (2024) 247-256. https://doi.org/10.1021/acs.accounts.3c00633.
[13] C. Guo, W. Zhou, X. Lan, Y. Wang, T. Li, S. Han, Y. Yu, B. Zhang, Electrochemical Upgrading of Formic Acid to Formamide via Coupling Nitrite Co-Reduction, J. Am. Chem. Soc. 144 (2022) 16006-16011. https://doi.org/10.1021/jacs.2c05660.
[14] N. Meng, J. Shao, H. Li, Y. Wang, X. Fu, C. Liu, Y. Yu, B. Zhang, Electrosynthesis of formamide from methanol and ammonia under ambient conditions, Nat. Commun. 13 (2022) 5452. https://doi.org/10.1038/s41467-022-33232-w.
[15] J. Zhu, J. Shao, B.-A. Shen, J. Chen, Y. Yu, S. Song, X.-B. Zhang, B. Zhang, B.-H. Zhao, Formamide Electrosynthesis from Methanol and Ammonia in Water over Pr-Doped MnO_2, JACS Au 3 (2023) 2987-2992. https://doi.org/10.1021/jacsau.3c00537.
[16] J.J. Roylance, K.-S. Choi, Electrochemical reductive amination of furfural-based biomass intermediates, Green Chem. 18 (2016) 5412-5417. https://doi.org/10.1039/C6GC01541G.
[17] S.D. Mürtz, N. Kurig, F.J. Holzhäuser, R. Palkovits, Reviving electrocatalytic reductive amination: a sustainable route from biogenic levulinic acid to 1,5-dimethyl-2-pyrrolidone, Green Chem. 23 (2021) 8428-8433. https://doi.org/10.1039/D1GC02513A.
[18] M. Zhang, S. Xu, M. Boubeche, D. Decarolis, Y. Huang, B. Liu, E.K. Gibson, X. Li, Y. Wang, H. Luo, C.R.A. Catlow, K. Yan, Designed TiS_2 nanosheets for efficient electrocatalytic reductive amination of biomass-derived furfurals, Green Chem. 24 (2022) 9570-9578. https://doi.org/10.1039/D2GC03234A.
[19] Y. Xiao, C.W. Lim, J. Chang, Q. Yuan, L. Wang, N. Yan, Electrocatalytic amino acid synthesis from biomass-derivable keto acids over ball milled carbon nanotubes, Green Chem. 25 (2023) 3117-3126. https://doi.org/10.1039/D3GC00265A.
[20] M. Li, Y. Wu, B.-H. Zhao, C. Cheng, J. Zhao, C. Liu, B. Zhang, Electrosynthesis of amino acids from NO and α-keto acids using two decoupled flow reactors, Nat. Catal. 6 (2023) 906-915. https://doi.org/10.1038/s41929-023-01012-4.
[21] J. Xian, S. Li, H. Su, P. Liao, S. Wang, Y. Zhang, W. Yang, J. Yang, Y. Sun, Y. Jia, Q. Liu, Q. Liu, G. Li, Electrocatalytic Synthesis of Essential Amino Acids from Nitric Oxide Using Atomically Dispersed Fe on N-doped Carbon, Angew. Chem. Int. Ed. 62 (2023) e202304007. https://doi.org/10.1002/anie.202304007.
[22] J. Xian, S. Li, H. Su, P. Liao, S. Wang, R. Xiang, Y. Zhang, Q. Liu, G. Li, Electrosynthesis of α-Amino Acids from NO and other NO_x species over CoFe alloy-decorated Self-standing Carbon Fiber Membranes, Angew. Chem. Int. Ed. 62 (2023) e202306726. https://doi.org/10.1002/anie.202306726.
[23] M.J. Hülsey, H. Yang, N. Yan, Sustainable Routes for the Synthesis of Renewable Heteroatom-Containing Chemicals, ACS Sustain. Chem. Eng. 6 (2018) 5694-5707. https://doi.org/10.1021/acssuschemeng.8b00612.
[24] X. Chen, S. Song, H. Li, G. Gözaydın, N. Yan, Expanding the Boundary of Biorefinery: Organonitrogen Chemicals from Biomass, Acc. Chem. Res. 54 (2021) 1711-1722. https://doi.org/10.1021/acs.accounts.0c00842.
[25] C. Galli, Radical reactions of arenediazonium ions: An easy entry into the chemistry of the aryl radical, Chem. Rev. 88 (1988) 765-792. https://doi.org/10.1021/cr00087a004.

[26] J. Lindley, Tetrahedron report number 163: Copper assisted nucleophilic substitution of aryl halogen, Tetrahedron 40 (1984) 1433-1456. https://doi.org/10.1016/S0040-4020(01)91791-0.
[27] N. Mori, H. Togo, Direct Oxidative Conversion of Primary Alcohols to Nitriles Using Molecular Iodine in Ammonia Water, Synlett 2005 (2005) 1456-1458.
[28] T. Oishi, K. Yamaguchi, N. Mizuno, Catalytic Oxidative Synthesis of Nitriles Directly from Primary Alcohols and Ammonia, Angew. Chem. Int. Ed. 48 (2009) 6286-6288. https://doi.org/10.1002/anie.200900418.
[29] T. Ishida, H. Watanabe, T. Takei, A. Hamasaki, M. Tokunaga, M. Haruta, Metal oxide-catalyzed ammoxidation of alcohols to nitriles and promotion effect of gold nanoparticles for one-pot amide synthesis, Appl. Catal. A 425-426 (2012) 85-90. https://doi.org/10.1016/j.apcata.2012.03.006.
[30] D.K.T. Yadav, B.M. Bhanage, Copper-Catalyzed Synthesis of Nitriles by Aerobic Oxidative Reaction of Alcohols and Ammonium Formate, Eur. J. Org. Chem. 2013 (2013) 5106-5110. https://doi.org/10.1002/ejoc.201300361.
[31] W. Yin, C. Wang, Y. Huang, Highly Practical Synthesis of Nitriles and Heterocycles from Alcohols under Mild Conditions by Aerobic Double Dehydrogenative Catalysis, Org. Lett. 15 (2013) 1850-1853. https://doi.org/10.1021/ol400459y.
[32] R.V. Jagadeesh, H. Junge, M. Beller, Green synthesis of nitriles using non-noble metal oxides-based nanocatalysts, Nat. Commun. 5 (2014) 4123. https://doi.org/10.1038/ncomms5123.
[33] S. Shang, L. Wang, W. Dai, B. Chen, Y. Lv, S. Gao, High catalytic activity of mesoporous Co–N/C catalysts for aerobic oxidative synthesis of nitriles, Catal. Sci. Technol. 6 (2016) 5746-5753. https://doi.org/10.1039/C6CY00195E.
[34] Y. Hu, S. Jin, Z. Zhang, L. Zhang, J. Deng, H. Zhang, One-step synthesis of nitriles by the dehydrogenation–amination of fatty primary alcohols over Cu/m-ZrO_2, Catal. Commun. 54 (2014) 45-49. https://doi.org/10.1016/j.catcom.2014.05.010.
[35] Y. Wang, S. Furukawa, Z. Zhang, L. Torrente-Murciano, S.A. Khan, N. Yan, Oxidant free conversion of alcohols to nitriles over Ni-based catalysts, Catal. Sci. Technol. 9 (2019) 86-96. https://doi.org/10.1039/C8CY01799A.
[36] Y. Wang, S. Furukawa, N. Yan, Identification of an Active NiCu Catalyst for Nitrile Synthesis from Alcohol, ACS Catal. 9 (2019) 6681-6691. https://doi.org/10.1021/acscatal.9b00043.
[37] N. Kiratzis, M. Stoukides, The Synthesis of Hydrogen Cyanide in a Solid Electrolyte Fuel Cell, J. Electrochem. Soc. 134 (1987) 1925-1929. https://doi.org/10.1149/1.2100791.
[38] N. Kiratzis, M. Stoukides, The synthesis of HCN in a solid electrolyte cell, J. Catal. 132 (1991) 257-262. https://doi.org/10.1016/0021-9517(91)90262-3.
[39] A. Raj, R.A. Rudkin, A. Atkinson, Cogeneration of HCN in a Solid Oxide Fuel Cell, J. Electrochem. Soc. 157 (2010) B719. https://doi.org/10.1149/1.3330704.
[40] Z. Fang, Y. Ding, M. Wang, L. Wang, F. Li, K. Fan, X. Wu, L. Sun, P. Zhang, Synthesis of nitriles by the electro-oxidative coupling of primary alcohols and ammonia on Pd nanoparticle-modified CuO nanowires in oxidant-free electrolytes under ambient conditions, Appl. Catal. B 337 (2023) 122999. https://doi.org/10.1016/j.apcatb.2023.122999.
[41] M. Osman, M.M. Hossain, S. Al-Khattaf, Kinetics Study of Ethylbenzene Alkylation with Ethanol over Medium and Large Pore Zeolites, Ind. Eng. Chem. Res. 52 (2013) 13613-13621. https://doi.org/10.1021/ie4016717.

[42] S. Siankevich, G. Savoglidis, Z. Fei, G. Laurenczy, D.T.L. Alexander, N. Yan, P.J. Dyson, A novel platinum nanocatalyst for the oxidation of 5-Hydroxymethylfurfural into 2,5-Furandicarboxylic acid under mild conditions, J. Catal. 315 (2014) 67-74. https://doi.org/10.1016/j.jcat.2014.04.011.
[43] S. Song, Y. Wang, N. Yan, A remarkable solvent effect on reductive amination of ketones, Mol. Catal. 454 (2018) 87-93. https://doi.org/10.1016/j.mcat.2018.05.017.
[44] Y. Wang, S. Furukawa, X. Fu, N. Yan, Organonitrogen Chemicals from Oxygen-Containing Feedstock over Heterogeneous Catalysts, ACS Catal. 10 (2020) 311-335. https://doi.org/10.1021/acscatal.9b03744.
[45] N.M. Adli, H. Zhang, S. Mukherjee, G. Wu, Review—Ammonia Oxidation Electrocatalysis for Hydrogen Generation and Fuel Cells, J. Electrochem. Soc. 165 (2018) J3130. https://doi.org/10.1149/2.0191815jes.
[46] Y. Tang, X. Li, H. Lv, D. Xie, W. Wang, C. Zhi, H. Li, Stabilized Co^{3+}/Co^{4+} Redox Pair in In Situ Produced $CoSe_2$−x-Derived Cobalt Oxides for Alkaline Zn Batteries with 10 000-Cycle Lifespan and 1.9-V Voltage Plateau, Adv. Energy Mater. 10 (2020) 2000892. https://doi.org/10.1002/aenm.202000892.
[47] P.M. Robertson, On the oxidation of alcohols and amines at nickel oxide electrodes: Mechanistic aspects, J. Electroanal. Chem. Interfacial Electrochem. 111 (1980) 97-104. https://doi.org/10.1016/S0022-0728(80)80079-9.
[48] Y. Huang, X. Chong, C. Liu, Y. Liang, B. Zhang, Boosting Hydrogen Production by Anodic Oxidation of Primary Amines over a NiSe Nanorod Electrode, Angew. Chem. Int. Ed. 57 (2018) 13163-13166. https://doi.org/10.1002/anie.201807717.
[49] W. Wang, Y. Wang, R. Yang, Q. Wen, Y. Liu, Z. Jiang, H. Li, T. Zhai, Vacancy-Rich $Ni(OH)_2$ Drives the Electrooxidation of Amino C−N Bonds to Nitrile C≡N Bonds, Angew. Chem. Int. Ed. 59 (2020) 16974-16981. https://doi.org/10.1002/anie.202005574.
[50] Y. Wang, Y.-Y. Xue, L.-T. Yan, H.-P. Li, Y.-P. Li, E.-H. Yuan, M. Li, S.-N. Li, Q.-G. Zhai, Multimetal Incorporation into 2D Conductive Metal–Organic Framework Nanowires Enabling Excellent Electrocatalytic Oxidation of Benzylamine to Benzonitrile, ACS Appl. Mater. Interfaces 12 (2020) 24786-24795. https://doi.org/10.1021/acsami.0c05094.
[51] Y. Ding, B.-Q. Miao, S.-N. Li, Y.-C. Jiang, Y.-Y. Liu, H.-C. Yao, Y. Chen, Benzylamine oxidation boosted electrochemical water-splitting: Hydrogen and benzonitrile co-production at ultra-thin Ni_2P nanomeshes grown on nickel foam, Appl. Catal. B 268 (2020) 118393. https://doi.org/10.1016/j.apcatb.2019.118393.
[52] W. Chen, C. Xie, Y. Wang, Y. Zou, C.-L. Dong, Y.-C. Huang, Z. Xiao, Z. Wei, S. Du, C. Chen, B. Zhou, J. Ma, S. Wang, Activity Origins and Design Principles of Nickel-Based Catalysts for Nucleophile Electrooxidation, Chem 6 (2020) 2974-2993. https://doi.org/10.1016/j.chempr.2020.07.022.
[53] M. Xiang, Z. Xu, Q. Wu, Y. Wang, Z. Yan, Selective electrooxidation of primary amines over a Ni/Co metal-organic framework derived electrode enabling effective hydrogen production in the membrane-free electrolyzer, J. Power Sources 535 (2022) 231461. https://doi.org/10.1016/j.jpowsour.2022.231461.
[54] M.T. Bender, K.-S. Choi, Electrochemical Dehydrogenation Pathways of Amines to Nitriles on NiOOH, JACS Au 2 (2022) 1169-1180. https://doi.org/10.1021/jacsau.2c00150.
[55] Y. Sun, H. Shin, F. Wang, B. Tian, C.-W. Chiang, S. Liu, X. Li, Y. Wang, L. Tang, W.A. Goddard, III, M. Ding, Highly Selective Electrocatalytic Oxidation of Amines to Nitriles Assisted by Water Oxidation on Metal-Doped α-$Ni(OH)_2$, J. Am. Chem. Soc. 144 (2022) 15185-15192. https://doi.org/10.1021/jacs.2c05403.

[56] X. Cao, Y. Wang, D. Tan, B. Wulan, J. Ma, W. Guo, J. Zhang, Stepwise dispersion of nickel species for efficient coupling of electrocatalytic redox reactions, Chem. Eng. J. 454 (2023) 140062. https://doi.org/10.1016/j.cej.2022.140062.
[57] A. Kapałka, A. Cally, S. Neodo, C. Comninellis, M. Wächter, K.M. Udert, Electrochemical behavior of ammonia at Ni/Ni(OH)$_2$ electrode, Electrochem. Commun. 12 (2010) 18-21. https://doi.org/10.1016/j.elecom.2009.10.026.
[58] M. Fleischmann, K. Korinek, D. Pletcher, The oxidation of organic compounds at a nickel anode in alkaline solution, J. Electroanal. Chem. Interfacial Electrochem. 31 (1971) 39-49. https://doi.org/10.1016/S0022-0728(71)80040-2.
[59] D. Giovanelli, N.S. Lawrence, L. Jiang, T.G.J. Jones, R.G. Compton, Electrochemical determination of sulphide at nickel electrodes in alkaline media: a new electrochemical sensor, Sens. Actuators B Chem. 88 (2003) 320-328. https://doi.org/10.1016/S0925-4005(02)00378-7.
[60] D. Jia, F. Li, L. Sheng, Q. Ren, S. Dong, S. Xu, Y. Mu, Y. Miao, Synthesis and assembly of ultrathin film of Ni(OH)$_2$ nanoparticles at gas/liquid interface, its high electrocatalytical oxidation toward bio-thiols and selective determination of cysteine, Electrochem. Commun. 13 (2011) 1119-1122. https://doi.org/10.1016/j.elecom.2011.07.013.
[61] H. Zhao, D. Lu, J. Wang, W. Tu, D. Wu, S.W. Koh, P. Gao, Z.J. Xu, S. Deng, Y. Zhou, B. You, H. Li, Raw biomass electroreforming coupled to green hydrogen generation, Nat. Commun. 12 (2021) 2008. https://doi.org/10.1038/s41467-021-22250-9.
[62] H.J. Schäfer, Oxidation of Organic Compounds at the Nickel Hydroxide Electrode, Electrochemistry I (1987). https://doi.org/10.1007/3-540-17871-6_13.
[63] M.T. Bender, Y.C. Lam, S. Hammes-Schiffer, K.-S. Choi, Unraveling Two Pathways for Electrochemical Alcohol and Aldehyde Oxidation on NiOOH, J. Am. Chem. Soc. 142 (2020) 21538-21547. https://doi.org/10.1021/jacs.0c10924.
[64] M.T. Bender, R.E. Warburton, S. Hammes-Schiffer, K.-S. Choi, Understanding Hydrogen Atom and Hydride Transfer Processes during Electrochemical Alcohol and Aldehyde Oxidation, ACS Catal. 11 (2021) 15110-15124. https://doi.org/10.1021/acscatal.1c04163.
[65] P. Parpot, A.P. Bettencourt, A.M. Carvalho, E.M. Belgsir, Biomass conversion: attempted electrooxidation of lignin for vanillin production, J. Appl. Electrochem. 30 (2000) 727-731. https://doi.org/10.1023/A:1004003613883.
[66] C.Z. Smith, J.H.P. Utley, J.K. Hammond, Electro-organic reactions. Part 60[1]. The electro-oxidative conversion at laboratory scale of a lignosulfonate into vanillin in an FM01 filter press flow reactor: preparative and mechanistic aspects, J. Appl. Electrochem. 41 (2011) 363-375. https://doi.org/10.1007/s10800-010-0245-0.
[67] C. Hansch, A. Leo, R.W. Taft, A survey of Hammett substituent constants and resonance and field parameters, Chem. Rev. 91 (1991) 165-195. https://doi.org/10.1021/cr00002a004.
[68] D.R. Weinberg, C.J. Gagliardi, J.F. Hull, C.F. Murphy, C.A. Kent, B.C. Westlake, A. Paul, D.H. Ess, D.G. McCafferty, T.J. Meyer, Proton-Coupled Electron Transfer, Chem. Rev. 112 (2012) 4016-4093. https://doi.org/10.1021/cr200177j.
[69] M.J. Chalkley, P. Garrido-Barros, J.C. Peters, A molecular mediator for reductive concerted proton-electron transfers via electrocatalysis, Science 369 (2020) 850-854. https://doi.org/10.1126/science.abc1607.
[70] J. Xu, J. Meng, Y. Hu, Y. Liu, Y. Lou, W. Bai, S. Dou, H. Yu, S. Wang, Electrocatalytic Lignin Valorization into Aromatic Products via Oxidative Cleavage of C_α–C_β Bonds, Research 6 (2023) 0288. https://doi.org/10.34133/research.0288.

[71] Y. Sang, H. Chen, M. Khalifeh, Y. Li, Catalysis and chemistry of lignin depolymerization in alcohol solvents - A review, Catal. Today 408 (2023) 168-181. https://doi.org/10.1016/j.cattod.2022.06.005.
[72] F. Li, Y.C. Li, Z. Wang, J. Li, D.-H. Nam, Y. Lum, M. Luo, X. Wang, A. Ozden, S.-F. Hung, B. Chen, Y. Wang, J. Wicks, Y. Xu, Y. Li, C.M. Gabardo, C.-T. Dinh, Y. Wang, T.-T. Zhuang, D. Sinton, E.H. Sargent, Cooperative CO_2-to-ethanol conversion via enriched intermediates at molecule–metal catalyst interfaces, Nat. Catal. 3 (2020) 75-82. https://doi.org/10.1038/s41929-019-0383-7.
[73] M. Irshad, H.-J. Chun, M.K. Khan, H. Jo, S.K. Kim, J. Kim, Synthesis of n-butanol-rich C_{3+} alcohols by direct CO_2 hydrogenation over a stable Cu–Co tandem catalyst, Appl. Catal. B 340 (2024) 123201. https://doi.org/10.1016/j.apcatb.2023.123201.
[74] I. Lauer, G. Philipps, S. Jennewein, Metabolic engineering of Clostridium ljungdahlii for the production of hexanol and butanol from CO_2 and H_2, Microb. Cell Factories 21 (2022) 85. https://doi.org/10.1186/s12934-022-01802-8.
[75] J. He, S.P. Burt, M. Ball, D. Zhao, I. Hermans, J.A. Dumesic, G.W. Huber, Synthesis of 1,6-Hexanediol from Cellulose Derived Tetrahydrofuran-Dimethanol with Pt-WOx/TiO_2 Catalysts, ACS Catal. 8 (2018) 1427-1439. https://doi.org/10.1021/acscatal.7b03593.
[76] Y. Jing, Y. Guo, Q. Xia, X. Liu, Y. Wang, Catalytic Production of Value-Added Chemicals and Liquid Fuels from Lignocellulosic Biomass, Chem 5 (2019) 2520-2546. https://doi.org/10.1016/j.chempr.2019.05.022.